AN ABSTRACT OF THE THESIS OF

ALAN NEAL STILLEY (Name) for the MASTER OF SCIENCE (Degree)

in CIVIL ENGINEERING (Major Department) presented on June 13, 1974 (Date)

Title: A MODEL STUDY OF FABRIC REINFORCED EARTH WALLS

Redacted for Privacy

Abstract approved: Dr. J. R. Bell

The concept of placing high strength linear reinforcements in a soil backfill to produce a vertical retaining structure is a recent idea that has been applied with success at a number of locations. Rational procedures have been developed for the design of these structures when the reinforcements consist of long metal straps. In certain situations advantages in construction and economy could be gained by replacing the metal straps with a continuous high strength fabric as reinforcement.

The purpose of this investigation was to examine the behavior of a number of fabric reinforced earth models and to determine if the design methods that have been applied to metal strap reinforced earth walls can be applied to fabric reinforced walls. The economic feasibility of fabric reinforced earth walls was also investigated.

The results of the model tests indicated that the design of fabric reinforced earth walls using methods developed for metal strap

reinforced walls produces conservative results. Further investigation is required to define the actual mechanism involved in fabric reinforced earth walls. The economic analysis indicated that fabric reinforced walls can be competitive with other types of retaining structures for low heights.

A Model Study of Fabric Reinforced Earth Walls

by

Alan Neal Stilley

A THESIS

submitted to

Oregon State University

in partial fulfillment of
the requirements for the
degree of

Master of Science

Completed June 1974

Commencement June 1975

APPROVED:

Redacted for Privacy

Professor of Civil Engineering
in charge of major

Redacted for Privacy

Head of Department of Civil Engineering

Redacted for Privacy

Dean of Graduate School

Date thesis is presented June 13, 1974

Typed by Mary Jo Stratton for Alan Neal Stilley

ACKNOWLEDGEMENTS

The author is indebted to Dr. J. R. Bell and Dr. W. L. Schroeder for their advice and guidance during the research and preparation of this thesis. Grateful acknowledgement also goes to Mr. R. F. Nesbitt and the Crown Zellerbach Corporation for providing the financial assistance that made this research possible.

TABLE OF CONTENTS

LIST OF TABLES

LIST OF FIGURES

LIST OF TERMS

Term	Description	Dimensions
B	Width of a reinforced earth wall.	inches or feet
C_u	Coefficient of uniformity.	dimensionless
d	Depth to a point in a reinforced earth wall.	inches or feet
F	Force in a reinforcement.	lb
F_b	Friction force at wall base.	lb
F_f	Friction force between soil and reinforcement.	lb
F_L	Loading plate friction force.	lb
F_n	Force in layer n of reinforcement.	lb
F_s	Sidewall friction force.	lb
F_t	Sum of the forces in the reinforcements.	lb
F_w	Friction force between wall and soil.	lb
F_x	Force in reinforcement at Point X.	lb
F_y	Force in reinforcement at Point Y.	lb
F_{max}	Maximum force in any reinforcement in a reinforced earth wall.	lb
f	Coefficient of friction between soil and reinforcement.	dimensionless
H	Height of a reinforced earth wall.	inches or feet
K_a	Active lateral earth pressure coefficient.	dimensionless
L	Total length of reinforcement.	inches or feet

Term	Description	Dimensions
L_e	Effective length of reinforcement resisting pullout.	inches or feet
ℓ	A length of reinforcement.	inches or feet
n	Number of layers of reinforcement in a reinforced earth wall.	dimensionless
P	Horizontal earth force against a wall.	lb
P'	Total earth force against a wall.	lb
Q	Vertical surcharge load on failure wedge.	lb
Q'	Inclined surcharge load on failure wedge.	lb
q	Unit surcharge load on reinforced earth wall.	lb/in^2
q_f	Unit surcharge load on reinforced earth wall at failure.	lb/in^2
R	Reaction on failure plane in a reinforced earth wall.	lb
S	Horizontal reinforcement spacing in a reinforced earth wall.	inches or feet
T	Variation in tensile force with length in a reinforcement.	lb/in
t	Force per unit width in a fabric reinforcement.	lb/in
t_s	Ultimate fabric strength per unit width.	lb/in
W	Weight of failure wedge.	lb
X	Vertical reinforcement spacing in a reinforced earth wall.	inches or feet

Term	Description	Dimensions
α	Angle of inclination of surcharge loading at failure.	degrees
γ	Unit weight of soil.	lb/ft^3
ΔF	Change in the force in a reinforcement in a certain length.	lb
$\Delta\sigma_3$	Increase in the equivalent confining stress.	lb/in^2
δ	Angle of friction between soil and wall.	degrees
ϵ	Strain in an element.	percent or in/in
θ	Angle from horizontal to failure plane.	degrees
ϕ	Angle of internal friction of soil.	degrees
σ	Normal stress on a surface.	lb/in^2
σ_h	Lateral earth pressure.	lb/in^2
σ_1	Major principal stress on a soil element.	lb/in^2
σ_3	Initial confining stress on a soil element.	lb/in^2
σ_{3e}	Effective confining stress on a soil element.	lb/in^2
τ	Shearing stress on a surface.	lb/in^2

A MODEL STUDY OF FABRIC REINFORCED EARTH WALLS

INTRODUCTION

The modern concept of reinforced earth was originally developed and applied to the construction of vertical earth retaining structures by a French engineer, Henri Vidal in the 1960's (9).[1] Although Vidal was the first to recognize the idea that reinforcements could be included in an earth mass to produce a vertical retaining structure, the concept of strengthening soil with fibers or rods has been recognized for years as evidenced by the construction of corduroy roads and the planting of trees to reduce soil erosion.

Reinforced earth can be defined as the combination of earth and reinforcements to produce a structure that is capable of resisting large lateral earth pressures. Reinforced earth walls, in the past, have been constructed of three components as shown in Figure 1. The main component of the wall is the soil backfill that makes up the mass of the wall and is placed around the reinforcements. The reinforcements are components that can withstand major tensile stresses. Reinforcements have typically consisted of thin metal straps that extend into the backfill. A skin or facing that is connected to the reinforcements is required at the front edge of the wall

---

[1]Number in parentheses refers to bibliography entry.

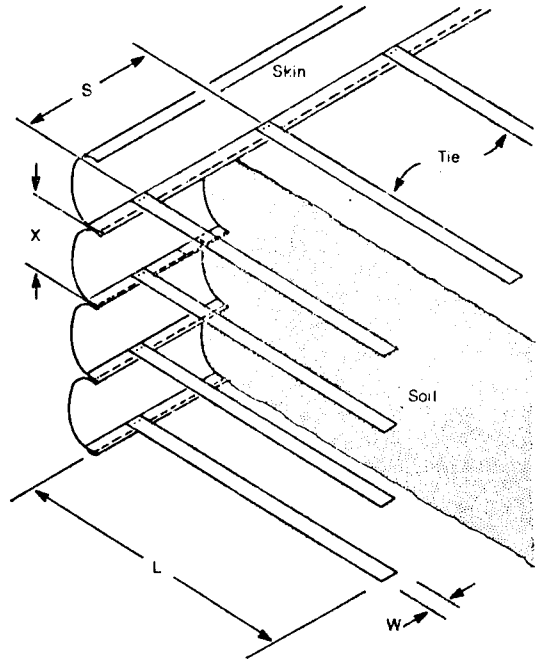

Figure 1. Components of a conventional reinforced earth wall (6).

to prevent local sloughing of the backfill. This face does not need to be particularly strong and curved thin-gauge metal sections or thin concrete slabs have typically been used to form wall faces.

The basic mechanism of reinforced earth is not well defined but it is thought that as the wall is formed, lateral outward movement of the face mobilizes a friction force between the backfill and the reinforcements. These friction forces produce tensile forces in the reinforcements. The reaction to the tensile forces in the reinforcements produces a confining stress in the soil particles in the immediate vicinity of the reinforcement. This induced confining stress,

which may be transferred between particles by the mechanism of arching, produces an increase in the shear strength of the soil.

From the geometry of reinforced earth walls and the mechanism involved, it can be seen that the ideal reinforcement should possess an optimum combination of a high tensile strength, a high coefficient of friction with the soil, a low cost, and resistance to corrosion or deterioration in a soil environment. A continuous layer of a high strength fabric may satisfy these requirements and might be feasible for use in reinforced earth walls.

The major advantages that would be expected from using a fabric in place of linear reinforcements in a reinforced earth wall are as follows. First, continuous fabric reinforcement would provide a large area to develop friction forces between the fabric and the soil. Combined with the fact that the coefficient of friction between a fabric and a soil is usually high, this would allow the full tensile strength of the fabric to be developed. Second, it may be possible to use the fabric to form the face of a reinforced earth wall. By using one continuous sheet, the fabric could be used as reinforcement in one layer and then lapped up around the face and used as reinforcement in the next higher layer. This would eliminate the need for a separate face element in construction. Third, the use of fabric reinforcement could be expected to facilitate construction methods. Fabric is generally easy to handle and could be placed by hand without the use

of heavy equipment. In addition, if the fabric was used to form the wall face, heavy face elements would be eliminated and there would be no need for connections between reinforcing and face. Finally, the use of continuous reinforcement could be expected to provide more soil arching action between reinforcement layers than would be possible using thin, widely spaced straps. This might provide a significant increase in the effective strength of the soil.

PURPOSE AND SCOPE OF INVESTIGATION

The study that is reported herein was undertaken to provide a preliminary indication of the feasibility of using continuous layers of fabric as reinforcement in reinforced earth walls. Since reinforced earth walls derive their stability from friction forces between the backfill and the reinforcements, this study was limited to the use of a granular non-cohesive sand backfill. Specifically, it was the purpose of this research to use small scale model reinforced earth walls as an aid in answering the following questions:

1. Are fabric reinforced earth walls structurally feasible?
2. Can design methods that have been applied to metal strap reinforced earth walls be applied to fabric reinforced earth walls?
3. Are fabric reinforced earth walls economically feasible?
4. What further research should be conducted to establish design methods?

A total of 13 fabric reinforced earth walls approximately one and one-half feet high were built and loaded to failure. This study reviews some of the current theories of behavior of reinforced earth and compares the observed behavior of the model walls with these theories. Finally, a brief economic analysis of fabric reinforced

earth walls is presented and an economic comparison with metal strap reinforced earth walls and conventional retaining walls is made.

LITERATURE REVIEW

The concept of the rational engineering design of reinforced earth is a relatively recent one. Therefore there is not a large historical background of studies of the problem. In recent years though, there have been several theories of the mechanism involved and some possible design methods published.

Vidal's Original Work

Basic research on the problem was first conducted by Henri Vidal (9). He recognized the fact that friction between the backfill and the reinforcements was the mechanism that provides stability to reinforced earth. If a section of reinforcement in contact with soil particles as shown in Figure 2 is examined, the tension force in the reinforcement is observed to vary over a certain length by the amount of friction, F_f, that is taking place between the soil and the reinforcement in that length. Over the length of reinforcement, ℓ, the force in the reinforcement varies by

$$\Delta F = F_x - F_y = F_f . \qquad [1]$$

For a reinforcement of unit width with a normal pressure, σ, acting on it and a coefficient of friction, f, between the soil and the reinforcement, the stability is insured if

$$\Delta F < 2\ell\sigma f . \qquad [2]$$

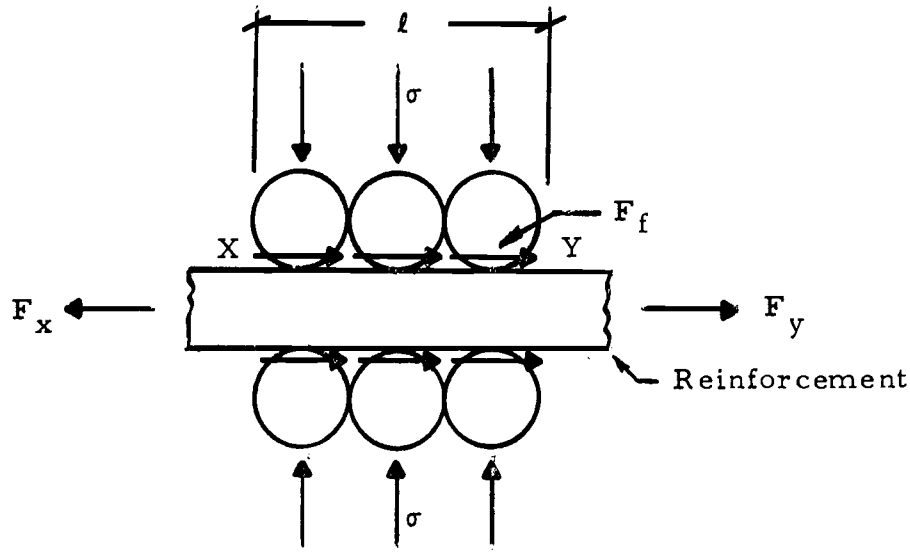

Figure 2. Soil particles in contact with a reinforcement.

If T is defined as the variation in tensile stress with length for a unit width of reinforcement

$$T = \Delta F / \ell . \qquad [3]$$

Substitution of Equation 2 into Equation 3 shows

$$T < 2\sigma f . \qquad [4]$$

If T can be limited to some value which is characteristic for a given reinforcement and soil at all points in a reinforced earth mass, then friction is developed without sliding. Actual application of the above concepts to practical design methods was not made clear by Vidal.

Vidal also examined the concept that friction between the soil and the reinforcement produced a confining stress that acted to

increase the shear strength of the soil. If a cohesionless soil with an angle of internal friction of ϕ conforms to the Mohr-Coulomb strength theory, the soil will have a strength envelope as shown in Figure 3 (c).

If the element of soil in Figure 3 (a) represents the stresses acting without reinforcement present, the corresponding Mohr circle of stresses will plot as C_a in Figure 3 (c). In this instance the strength envelope intersects Mohr's circle and a failure would occur. In Figure 3 (b), the reaction to a reinforcement in the soil element provides a lateral confining stress. If this confining stress is greater than $K_a\sigma$ (where $K_a = \tan^2 [45^\circ - \phi/2]$), the Mohr circle will plot below the strength envelope and the element will be stable. The Mohr circle of stresses is plotted for the condition where the induced lateral stress is equal to $K_a\sigma$ as curve C_b in Figure 3 (c). Application of this principle requires that some assumption be made about the variation in lateral stress with distance from the reinforcing element. It is logical to assume that the manner of transmission is by arching between the reinforcements but again Vidal was unclear as to how these principles could be applied in a practical design method.

Design Methods Based on Lateral Earth Pressure Theories

It is possible to apply the concepts of lateral earth pressure as developed for the design of conventional retaining structures to the

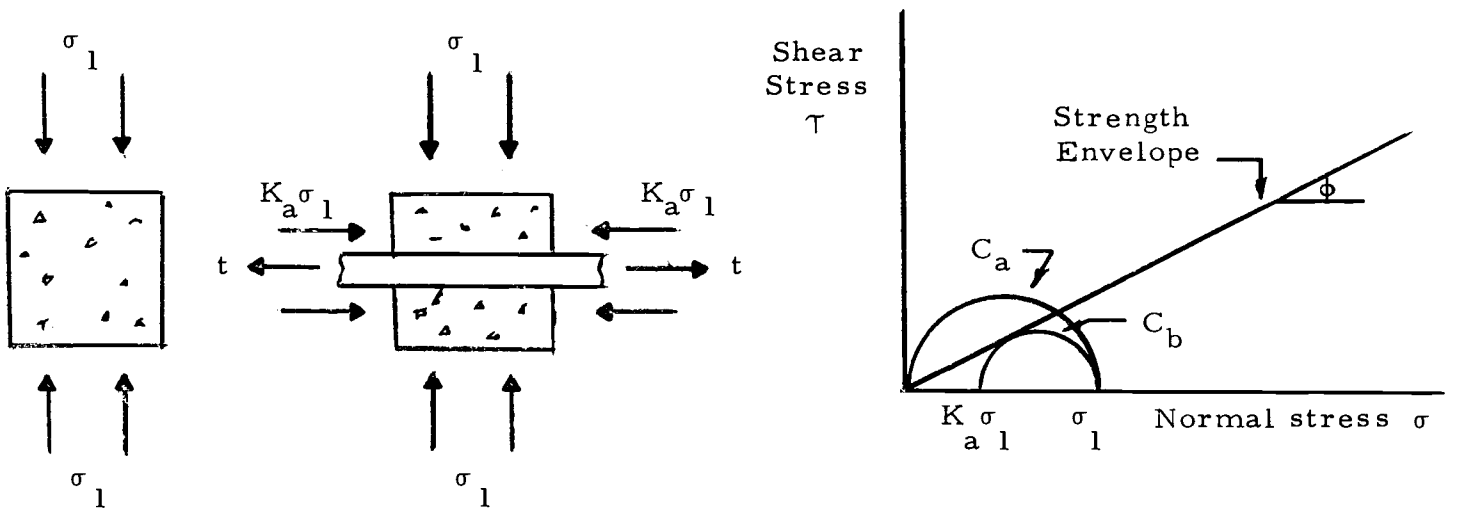

Figure 3. Stresses acting on a unit of soil and corresponding circles of stress.

design of reinforced earth walls. This method of design has been investigated by Lee et al. (5).

One analysis assumes that the lateral wall movement will be sufficient to put the sand contained in wedge ABC (Figure 4 [a]) into a Rankine state of active plastic equilibrium. With this assumption, the lateral earth pressure against the wall increases linearly with depth. The lateral earth pressure at any depth, d, below the top of the wall is given by

$$\sigma_h = K_a \gamma d \qquad [5]$$

where K_a is the active lateral earth pressure coefficient and γ is the unit weight of the soil. The failure surface AB slopes upward at an angle of θ to the horizontal.

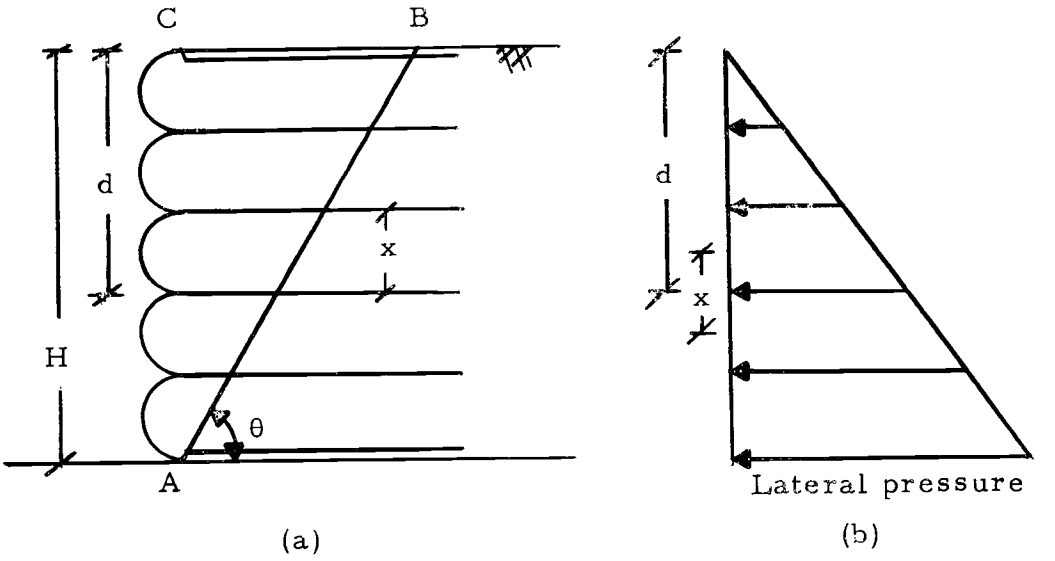

Figure 4. Dimensions involved in lateral earth pressure design.

Lee recognized that there are two modes of failure of a reinforced earth wall. First, the wall may fail due to the reinforcements breaking in tension. Second, the wall may fail by the reinforcements pulling out.

In the reinforcement failure analysis it is assumed that the tension in any reinforcement increases from a value of zero at the free end to a maximum at the wall face. As with retaining wall design, the Rankine earth pressure or the Coulomb earth pressure theory can be applied. Specifically, there are three design methods that have been applied. These are the Rankine method, the Coulomb force method, and the Coulomb moment method.

If the Rankine earth pressure theory is applied to a vertical wall with a level backfill the lateral earth pressure coefficient, K_a, is given by $\tan^2(45 - \phi/2)$, and the failure surface, AB, slopes upward at an angle of $\theta = 45 + \phi/2$. The Rankine method of reinforced wall design assumes that the tension in any one reinforcement can be calculated by multiplying the lateral stress at that level times the wall area that that reinforcement must support. If the vertical reinforcement spacing is X and the horizontal spacing is S, it can be seen from Figure 4 (b) that a reinforcement at level d in the wall must support a force of $K_a \gamma dSX$. If the reinforcement spacings, S and X remain constant throughout a wall, the maximum reinforcement tension will occur at the bottom of the wall and will be given by

$$F_{max} = K_a \gamma HSX \qquad [6]$$

The Coulomb earth pressure theory is a more general theory and accounts for the effects of wall friction. Specifically, the Coulomb design methods differ from the Rankine design method in two ways. First, the Coulomb earth pressure theory is applied. Second, the Coulomb methods consider the overall stability of the wall and not just the stability of one reinforcement. At failure, the wedge ABC shown in Figure 5 (a) is in equilibrium under the forces, W, the weight of the wedge, R, the reaction on the sliding surface AB, F_t, the sum of the forces in the reinforcements and F_w, the friction between the wall and the backfill. This assumes that the reinforcement tension acts directly on the wall face and does not influence the failure wedge.

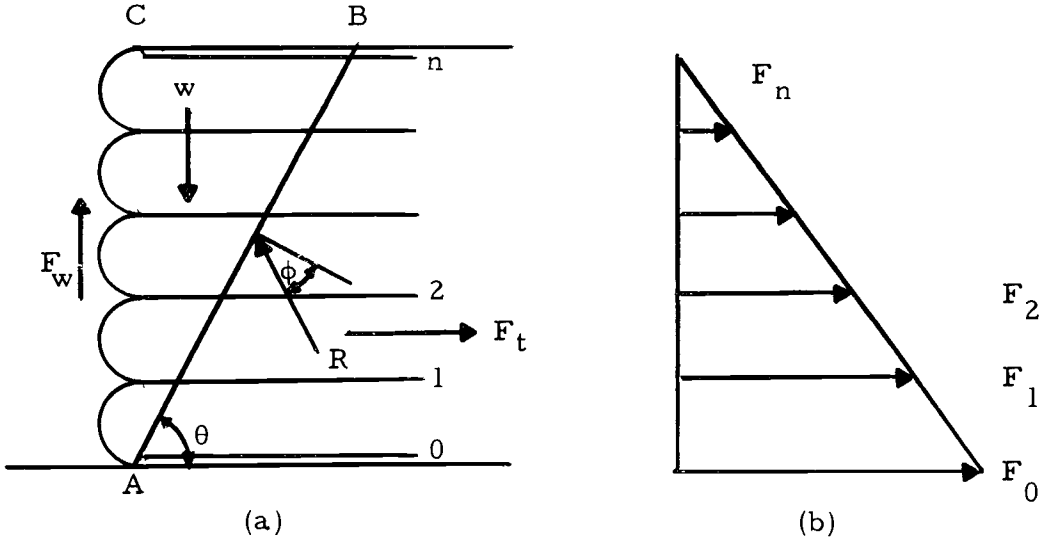

Figure 5. Forces acting on a reinforced earth wall.

The Coulomb force method assumes the reinforcement forces vary linearly with depth as shown in Figure 5 (b), and calculates the tension force in the reinforcements by equating horizontal forces. If n indicates the number of layers of reinforcement, and K_a is Coulomb's earth pressure coefficient, it can be shown (5) that the maximum reinforcement force occurs at the bottom of the wall and is given by

$$F_{max} = \frac{n}{n+1} K_a \gamma HSX \qquad [7]$$

The Coulomb moment method calculates the tension force in the reinforcements by equating the sum of the moments about the toe of the wall. Again the maximum tie force occurs at the bottom of the wall and is given by

$$F_{max} = \frac{n^2}{n^2 - 1} K_a \gamma HSX \qquad [8]$$

In the pull out analysis, it is necessary to insure that enough reinforcements are embedded far enough to resist the pullout force. Lee suggested that only the length of reinforcement that extends behind the failure plane be used to resist the pullout force. Thus in Figure 6, only the length, L_e, of reinforcement behind the failure plane AB would be used to resist pullout.

If L is the total length of the reinforcements, the effective length to resist pullout at any depth, d, would be given by

$$L_e = L - \frac{(H - d)}{\tan \theta} \qquad [9]$$

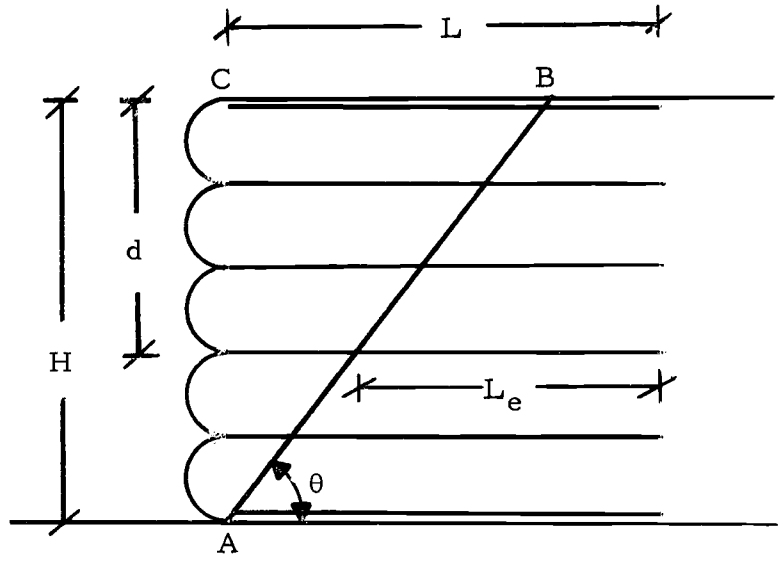

Figure 6. Effective length of reinforcement to resist pullout.

If the coefficient of friction between the reinforcements and the soil is known, it is possible to determine a factor of safety against pullout by each of the three previously described methods (5).

Equivalent Confining Stress Concept

Yang has studied the idea that fabric reinforcements introduce an increase in the confining stress of a soil mass (11). He developed a semi-empirical approach by analyzing the results of triaxial compression tests on sand samples reinforced with layers of fabric. He noted that the strength of triaxial sand samples increases considerably when they are reinforced with fabric layers. He also noted

that this strength increase depends on the ratio of the distance between reinforcements to the diameter of the sample and the strength and surface characteristics of the reinforcements. It was assumed that the value of the lateral earth pressure coefficient, K_a, remained unaffected by the presence of reinforcements. The equivalent confining stress was then calculated from the triaxial data by multiplying the peak deviator stress times the lateral earth pressure coefficient. He then defined the equivalent confining stress increase as the difference between the equivalent confining stress and the actual initial applied confining stress. A generalized plot of the equivalent confining stress increase versus the initial confining stress for one reinforcement spacing is shown in Figure 7.

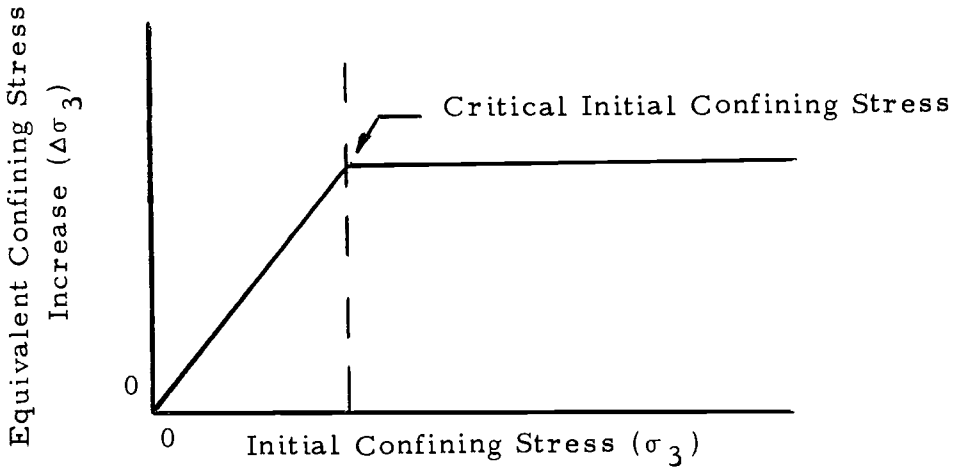

Figure 7. General relationship between initial confining stress and equivalent confining stress increase for constant reinforcement spacing.

As can be seen from Figure 7, the equivalent confining stress increase rises with rising initial confining stress until a critical initial confining stress is reached. Above this confining stress, the equivalent confining stress remains constant. Below this critical confining stress the triaxial samples failed by sliding between the sand and the fabric and above this stress, the samples failed by tearing of the fabric.

This approach is similar to Vidal's concept of lateral confining stress resulting from the reaction to reinforcement tension as illustrated in Figure 3. The equivalent confining stress is composed of the confining stress induced by the presence of the reinforcement and the natural ambient stress level. If t is the force per unit width in the reinforcement and σ_3 is the initial confining stress that would be present without reinforcement, the equivalent confining stress is given by

$$\sigma_{3e} = t/X + \sigma_3 . \qquad [10]$$

It is possible to relate the major principal stress, σ_1, which in this case is the vertical stress, to the effective confining stress, σ_{3e}, by the relation

$$\sigma_{3e} = \sigma_1 K_a \qquad [11]$$

Substitution of Equation 10 into Equation 11 gives

$$t/X + \sigma_3 = \sigma_1 K_a \qquad [12]$$

From Equation 12 it can be seen that if t is limited to the strength of the reinforcement and if the relationships for t/X and σ_3 can be defined, a maximum vertical stress and hence a maximum wall height for any reinforcement spacing can be specified.

Examination of Equation 12 shows that if σ_3 is zero this method reduces to the Rankine design method as described previously. This is the case at the contact between the sand and the facing. In this case the reinforcement tension, F, is given by the product of t and S and the vertical stress, σ_1, is given by γH. Substitution of these values with σ_3 equal to zero into Equation 12 yields Equation 6.

Yang's results essentially show that the benefit of the reinforcement increases as the friction increases until the full strength of the reinforcement is mobilized. Beyond that point, increasing friction does not further reinforce the soil. The equivalent confining stress theory tends to confirm that the active earth pressure theories should provide an adequate basis for the design of reinforced earth walls.

Various attempts have been made to confirm the validity of the reinforced earth theories experimentally. Lee constructed a number of model walls reinforced with metal straps (5). He observed that the lateral stress theory worked well in predicting model wall failures. He also found that the failure surfaces in the models were curved upward somewhat but that the deviation from the straight line assumption was slight. He further noted that his models failed by

breaking of the ties at the face. In 1972, the first reinforced earth embankment in the United States was constructed on Route 39 in Los Angeles County, California. This embankment was instrumented and monitored during and after construction by the California Division of Highways (2). They found that generally, the reinforced earth embankment performed according to the lateral stress theory with one exception. The stresses in the metal reinforcing straps increased from the face into the soil, reached a maximum at some point in the reinforced mass and then decreased. The point of maximum stress was located at approximately the point where the potential failure plane crossed the reinforcement. They found that reinforcement stresses could be predicted near the face of the wall using the coefficient of active earth pressure while the coefficient of earth pressure at rest more accurately predicted the maximum stresses near the failure plane.

LABORATORY STUDIES

Scheme

The construction of small scale model walls was selected as the most practical means of investigating fabric reinforced earth walls for this study. This necessitated the selection of a fabric for reinforcement and the design of an apparatus in which to construct and fail the models. It was decided to construct the model walls in a plywood and Plexiglas box. The box would contain the sand and behavior of the wall could be viewed through the Plexiglas during loading. The main consideration in selecting a fabric for reinforcement was the fabric strength. Theoretically, if a very low strength fabric was used, the model walls could be constructed so that they would fail under their own weight. This would eliminate the need for an external loading device. A number of fabrics were investigated but none could be found with a low enough strength to cause the wall to fail under its own weight. A non-woven polypropylene fabric was finally selected for reinforcement and strength tests indicated that moderate surcharge loading would be required to fail the model walls.

The model walls used in this study were not analyzed as scale models. The walls were analyzed as structures and dimensional analysis was not applied in selecting sizes. The criteria for the

selection of the model apparatus were as follows:

1. The model walls had to be small enough so that the volume of sand to be handled was reasonable.
2. The width to height ratio of the model walls had to be high enough to reduce the effect of side wall friction and arching between the sides.
3. The box had to be strong enough to resist the forces necessary to fail the model walls.
4. The apparatus used to place the sand had to reproduce constant sand densities throughout the wall.

Model Apparatus

The apparatus used to construct and test the model walls consisted of three items--a box to contain the walls, a placement system for the sand, and a loading device for applying surcharges.

The box was constructed with 3/4 inch thick Plexiglas sides and 3/4 inch thick plywood ends and bottom. The inside dimensions of the box were 24 inches wide, 36 inches long, and 18 inches high.

The sand placement system that was selected consisted of a commercial lawn spreader arranged on angle iron rails above the box. Walker and Whitaker (10) have reported using a similar device with good results. The spreader consisted of a rotary feed system that was connected to the axle. The volume of sand released was

controlled by a variable opening as shown in Figure 8. The width of the sand curtain that this spreader produced was 16 inches. The spreader was arranged on removable angle iron rails that were bolted over one end of the box so that it could be moved transverse to the length of the box. Previous studies (3) with the sand that was used in this study indicated that free-fall placement produced constant densities if the rate of placement was constant and if the height of fall was over 18 inches. For this reason, the spreader rails were placed at 22 inches above the top of the box. The assembled box and spreader are shown in Figure 9.

This system produced model walls in one end of the box that were 16 inches deep, 24 inches wide, and up to 18 inches high.

A hydraulic loading frame was selected for applying the surcharge to the models. The frame was about 15 feet high and after the walls were formed in the box, the spreader and rails were removed and the box was rolled under the frame for loading. The capacity of the device on the load range used was 6000 pounds, and loads on the model could be read to five pounds. The load was transferred from the machine to the model through a roller assembly that rested on two steel plates that were 23 inches by 15 inches in size. The bottom steel plate was 1/8 inch thick and the bottom of the plate was greased with 1/4 inch of grease to reduce friction between the loading plate and the sand. The upper steel plate was 1/4 inch thick.

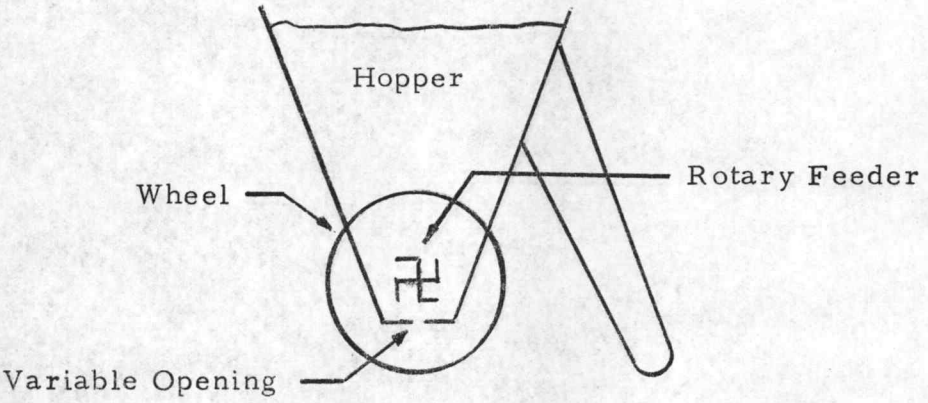

Figure 8. Profile view of sand spreading apparatus.

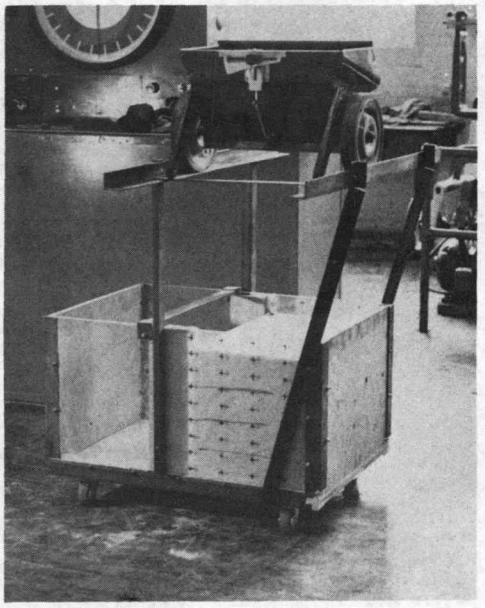

Figure 9. Model box with sand spreader assembled.

Two types of facing were used on the models. The first was 5/8 inch thick grooved plywood strips. The height of each strip corresponded to the vertical spacing between reinforcements. One sheet of fabric reinforcement was stapled to the top of each plywood strip. The plywood strips were held in place by guides that were bolted to the inside of the box while the wall was being formed. The guides were removed for testing. The second type of facing used was the reinforcing fabric. In these tests a metal semi-circular form was fixed across the box to hold the fabric up along the face while the wall was being formed. These forms were removed for testing.

Material Properties

The sand used to construct the model walls in this study was processed from a plastering sand known commercially as Del-Monte sand. The sand particles were angular in shape, white in color and composed primarily of quartz grains with a small amount of mica. The gradation curve for the sand used is shown in Figure 10.

Minimum density of the sand was determined by placement of the sand in a calibrated container under water. Maximum density of the sand was determined by repeated vibration of a four inch proctor mold filled with sand. A summary of the sand properties is presented in Table 1.

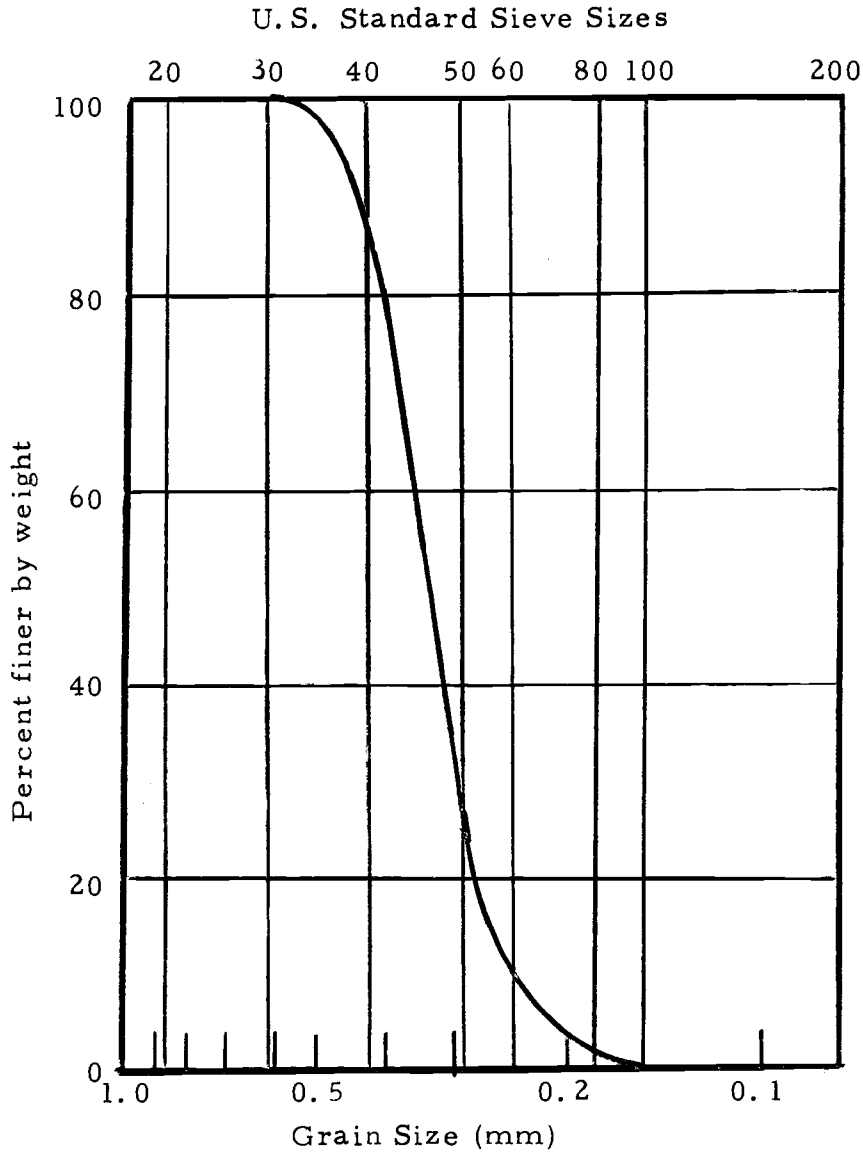

Figure 10. Sand gradation curve.

Table 1. Sand properties.

Coefficient of Uniformity (C_u)	Minimum Density (lb/ft^3)	Maximum Density (lb/ft^3)
1.2	80.7	99.1

The spreader used in this study had a variable opening that controlled the rate of flow of sand out of the bottom of the hopper. A scale on the hopper indicated the opening and read zero when the opening was closed and 20 when at its widest opening. It was found that sand densities in the model walls were dependent on the flow rate of the sand from the hopper and hence on the spreader opening. A constant spreader opening of eight was selected as the most convenient and was used for the construction of all models. Sand densities were determined in the model by raining sand from the spreader into two calibrated cylinders constructed of 20 gauge aluminum. The cylinders were five inches in diameter and about two and one-half inches in height and were formed to a knife edge around the lip to minimize disturbance. Table 2 presents the results of the density tests.

Examination of Table 2 indicates that the sand densities increased somewhat with depth in the wall although the maximum difference in observed densities was 1.4 lb/ft^3. This difference was not considered significant and an average of the densities in Table 2

Table 2. Results of density tests.

Location of Cylinder		Density (lb/ft^3)	Relative Density %
Below Spreader (in.)	Lateral Position		
40[a]	Cntr.	96.9	90.0
40[a]	N. Edge	97.5	92.8
37	Cntr.	97.2	91.4
34	S. Edge	96.6	88.6
34	Cntr.	96.8	89.6
31	W. Edge	96.7	89.1
27	E. Edge	96.5	88.2
25	S. Edge	96.3	87.3
25	S. Edge	96.2	86.8
24[b]	N. Edge	96.1	86.3

[a]Bottom of wall

[b]Top of wall

of 96.7 lb/ft^3 was used for all calculations. This gives a relative density of 89.1%. A series of vacuum triaxial tests were run on the sand at this density and they indicated an angle of internal friction of 38°.

The fabric used for reinforcement in this study was a synthetic, non-woven continuous filament type of web made of isotactic polypropylene. It weighed 1/2 ounce per square yard and came on a roll 24 inches wide. It was white in color, quite flexible, and approximately 10 mils in thickness.

The fabric exhibited different strength properties in the length-roll direction than it did in the cross-roll direction. For this reason, all of the model tests were conducted with the cross-roll direction of the fabric reinforcement parallel to the face of the wall and the strength characteristics of the fabric were determined from pulling tests in the length-roll direction. Strength characteristics of the fabric were determined by suspending weights from a six inch wide, 10 inch long specimen. The weights were applied in one pound increments and elongation in the vertical direction and contraction in the horizontal direction was measured. Figure 11 shows a typical stress-strain curve for the fabric and Table 3 lists the results of a number of strength tests.

Examination of Table 3 indicates that there is some variation in the strength of the fabric. The average of the strengths in Table 3 is 1.40 lb/in and the maximum variation from the average is about 16 percent. This average value was used for all calculations in this study and periodic strength tests during model construction confirmed this value.

Four different friction angles were considered important for analysis and measured. First, the angle of friction between the sand and the fabric was necessary for pullout calculations. Second, the angle of friction between the sand and plywood was necessary for calculation of wall friction. Third, the angle of friction between the sand

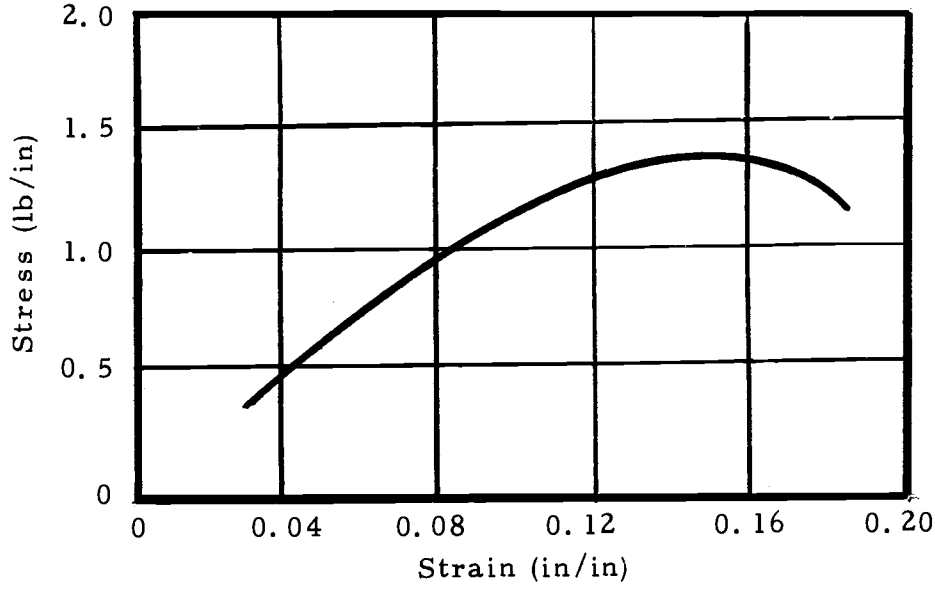

Figure 11. Typical fabric stress-strain curve.

Table 3. Fabric strength properties.

Test No.	Failure Strength (lb/in)	Percent Elongation at Failure
1	1.48	14.5
2	1.45	16.0
3	1.42	15.5
4	1.18	14.0
5	1.35	17.0
6	1.37	18.0
7	1.40	16.5
8	1.32	14.0
9	1.48	17.5
10	1.51	18.0

and Plexiglas was required for sidewall friction calculations and fourth, a friction angle between the sand and the greased loading plate was necessary. Two different types of grease were used on the loading plate. A sodium base grease was used for part of the tests and a barium base grease was used for the rest. Friction tests with both types produced the same results. The device used to measure the coefficients of friction consisted of a small plate mounted on ball-bearing wheels that ran along a track beneath a fixed two and one-half inch diameter ring. The material to be tested was attached to the plate and the ring was filled with sand and weights were placed on top of the sand to apply vertical loads. A hand-turned crank and worm-screw applied the horizontal force through a proving ring to move the plate relative to the ring. The results of the friction tests are presented in Table 4.

Table 4. Results of friction tests.

Friction Angle Between	Magnitude of Friction Angle
Sand and Fabric	38^{o}
Sand and Plywood	15^{o}
Sand and Plexiglas	11^{o}
Sand and Greased Plate	5^{o}

Test Procedure

The fabric reinforced earth models were constructed by raining sand from the spreader into the box. For the models with plywood facing, a grid system was drawn on the fabric and one sheet of fabric was stapled onto the top of each section of plywood as shown in Figure 12. One section of plywood at a time was placed in the guides inside the box. The fabric layer was then folded over the top of the plywood strip and sand was rained to the reinforcement level by moving the spreader over the box. The fabric layer was then spread over the sand, the next plywood facing was inserted and the process was repeated.

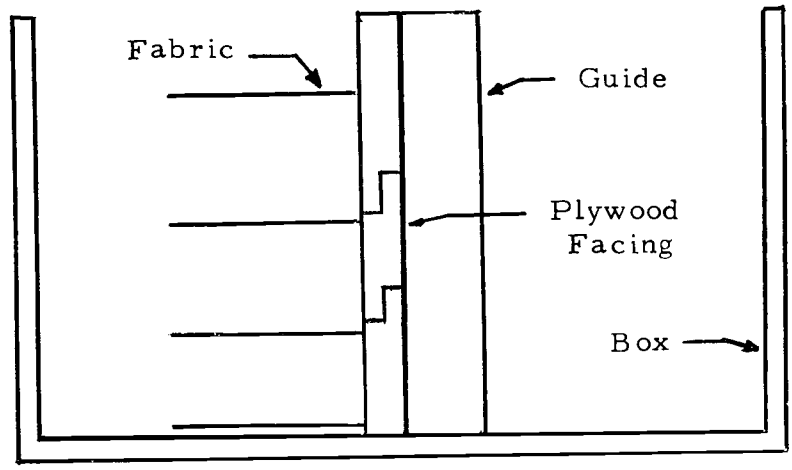

Figure 12. Plywood-faced model diagram.

The fabric-faced models were constructed with the aid of semi-circular sheet metal forms that fit in a guide on the inside of the box. A metal form was placed in the guide and a layer of fabric was laid out to the point of embeddment in the model and folded over the outside of the form. Sand was then rained to the top of the form and the fabric was folded back into the wall. This process was repeated until the desired wall height was reached. It was impossible to rain sand into the semi-circular outer face of the walls and sand was placed in this area by hand. In all of the models, the location of the fabric was marked with a thin layer of colored sand visible through the Plexiglas sides of the box.

After the model was formed, the sand spreader and facing guides were removed from the box and a greased loading plate was placed on top of the model. The box was then rolled under the loading frame. A load was then applied to the model and vertical and horizontal movements of the wall were recorded. The rate of loading for all models was maintained at a constant value. Deformation and load readings were taken until the model failed. The failure surface through the colored sand lenses, if evident, was then marked on the plexiglass. The sand was carefully taken out of the box with a vacuum recovery system and the fabric was removed.

Test Results

A total of 13 model tests were run for this study. Four elements of the model construction were selected as variables. These variables were as follows:

1. The type of model facing, plywood or fabric.
2. The vertical reinforcement spacing.
3. The horizontal reinforcement length.
4. The reinforcement strength, one or two layers of fabric.

A description of each of the models is listed in Table 5.

The arrangement of the fabric reinforcements in the plywood-faced model tests is shown in Figure 13. For these tests, a layer of sand equal to one-half of the vertical spacing between reinforcement layers was placed between the top reinforcement and the loading plate. Test 1A was the only exception as the loading plate was placed directly on the top layer for this test.

The arrangement of the reinforcement for the fabric-faced model Test 11A is shown in Figure 14 (a) and the arrangement for Tests 12A and 13A is shown in Figure 14 (b). For Tests 12A and 13A, a fabric overlap between layers equal to the vertical spacing between layers was adequate to prevent pullout of the individual layers.

The quantities that were measured in the model tests were the vertical load on the model, the rate of loading, the vertical deflection

Table 5. Model descriptions.

Model No.	Type of Facing	Height of Wall (in.)	Vertical Reinforcement Spacing (in.)	Fabric Sheets per Layer (no.)	Reinforcement Length (in.)
1A	plywood	16	4	1	10
2A	plywood	18	4	1	10
3A	plywood	18	4	1	7
4A	plywood	18	4	1	7
5A	plywood	18	4	1	10
6A	plywood	18	4	1	4.5
7A	plywood	18	4	2	10
8A	plywood	18	4	2	7
9A	plywood	16.5	3	1	7
10A	plywood	16.5	3	2	7
11A	fabric	16	4	2	7
12A	fabric	16	4	1	7
13A	fabric	16	4	1	7

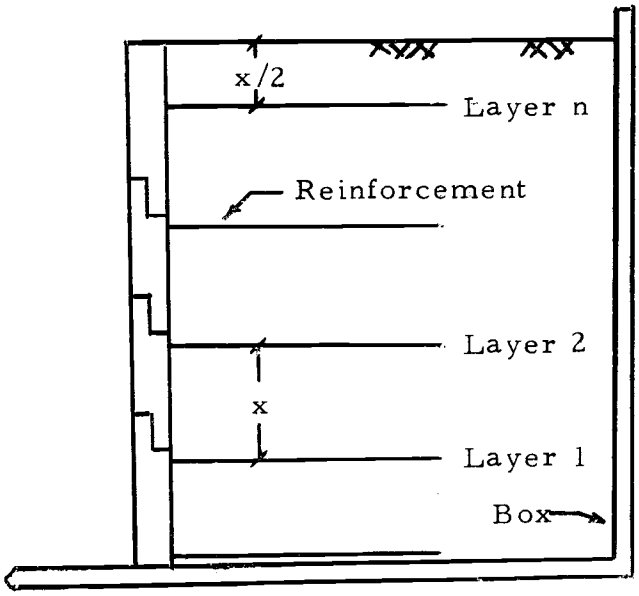

Figure 13. Arrangement of reinforcements for plywood-faced models.

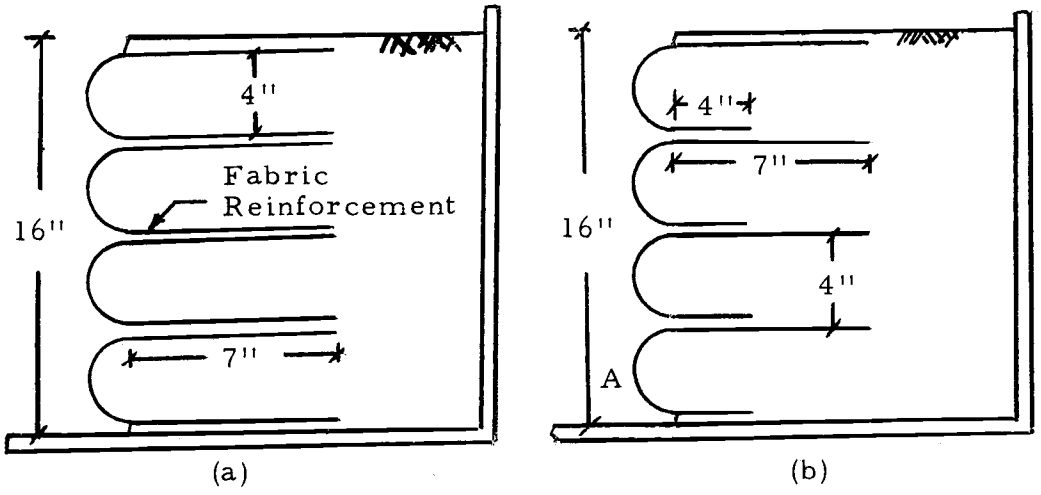

Figure 14. Arrangement of fabric in fabric-faced models.

of the top of the wall, the angle of inclination of the loading plate at failure, the horizontal movement of the wall face, and the angle of inclination from the horizontal to the soil failure plane. The results of the model tests are listed in Table 6.

The models that failed by breaking of the reinforcement did not fail suddenly. The load on the model reached a maximum and then decreased slowly as vertical and horizontal deflections became excessive. This maximum load was defined as the failure load. The loading head tilted somewhat during loading, and therefore the measured vertical deflection of the loading head represents an average vertical deflection. The stress-strain curves for each of the model tests are included in the Appendix. Most of the models displayed a definite failure plane as indicated by offsetting of the colored sand lenses. This plane was generally well defined near the bottom of the model and less evident near the top. Some of the failure planes appeared to be curved slightly upward. Figure 15 shows a model after failure.

The lower two or three fabric reinforcement layers usually displayed tearing that was parallel to the face of the wall. Figure 16 shows the fabric reinforcement from model Test 2A.

The fabric-faced models failed by a tearing of the fabric face for each layer. Tearing occurred at point A in Figure 14 (b) and was evident at the same location for each of the higher layers. There was

Table 6. Model test results.

Model No.	Type of Failure	Failure Load (lb)	Vertical Deflection at Failure (% of wall height)	Horizontal Movement of Wall Top at Failure (% of wall height)	Average Loading Rate (lb/min)	Approximate Angle of Inclination of Loading Plate at Failure (degrees)	Approximate Angle of Inclination of Failure Plane (degrees)
1A	Breaking	2390	4.6	9.4	65	6	60
2A	Breaking	2175	4.6	11.1	67	7	58
3A	Breaking	1530	5.8	8.3	55	8	65
4A	Breaking	1425	5.0	9.7	46	7	67
5A	Breaking	1950	4.8	10.2	59	5	65
6A	Pullout	310	1.7	-	48	-	-
7A	None	>6000	-	-	81	-	-
8A	Breaking	3570	8.9	9.9	78	6	62
9A	Breaking	2420	5.5	8.6	67	7	60
10A	Breaking	4890	9.1	10.4	75	6	59
11A	None	>6000	-	-	70	-	-
12A	Breaking	3250	11.8	13.8	73	7	65
13A	Breaking	3730	13.8	16.7	81	6	60

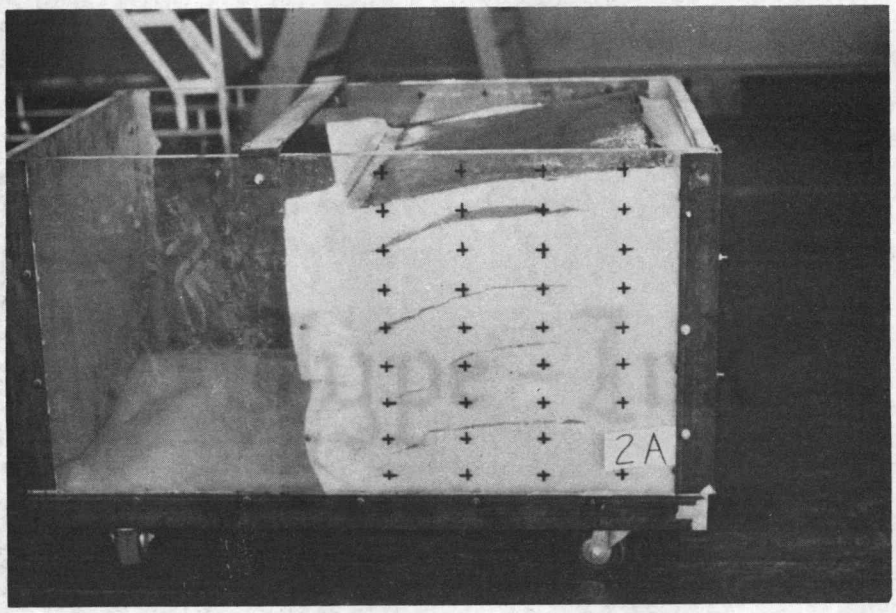

Figure 15. Model after failure (grid system two inches by four inches).

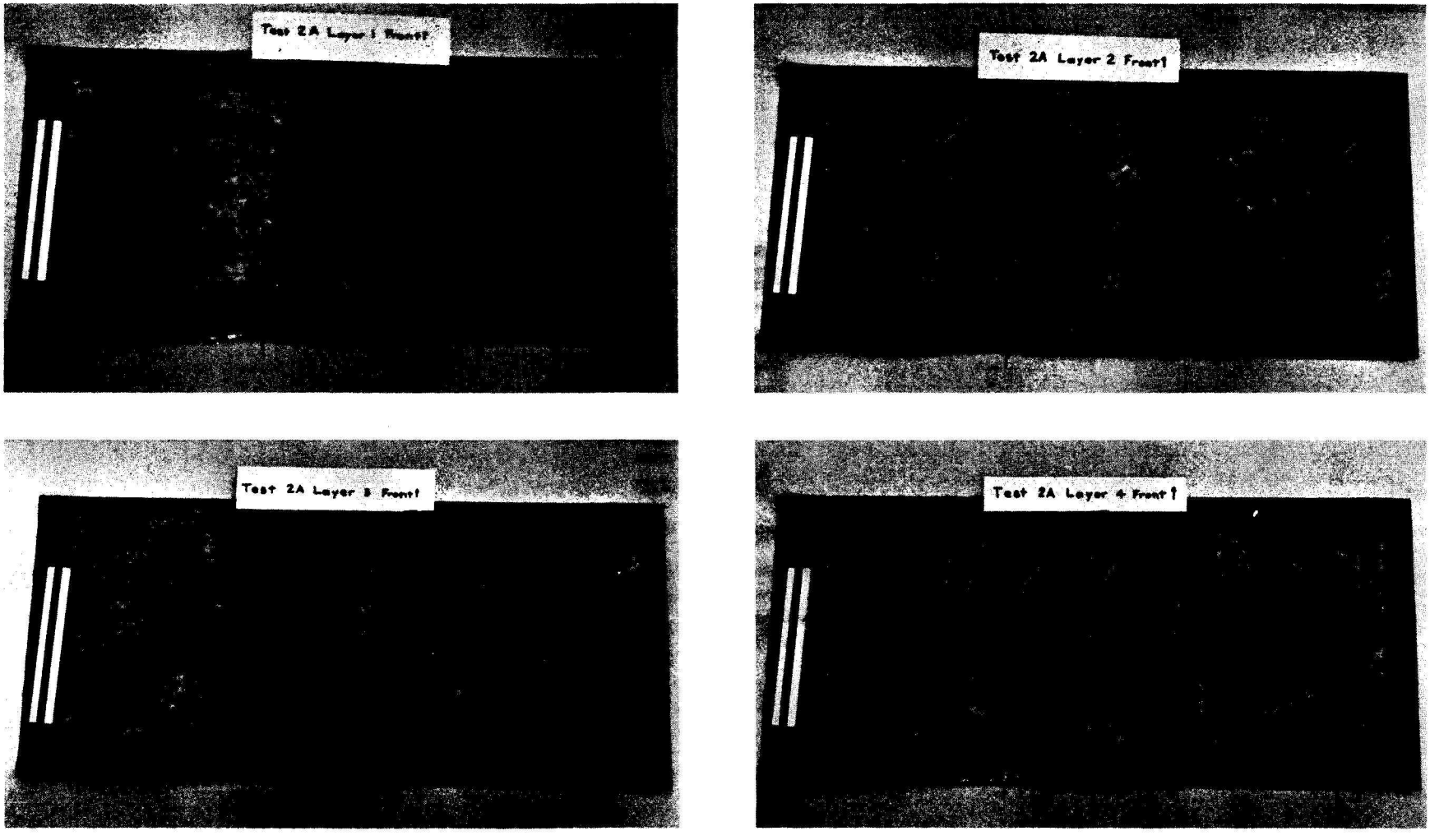

Figure 16. Model reinforcement layers after testing (grid system two inches by two inches).

also tearing of the reinforcement in the region of the failure plane similar to the plywood-faced models. Failure of the fabric-faced models was much more abrupt than for the plywood-faced models although neither type that failed by breaking of the reinforcements completely collapsed at failure.

The plywood model facing generally deformed as shown in Figure 17. The top of the wall at C moved outward approximately 10 percent of the wall height and the bottom wall strip remained fixed at A.

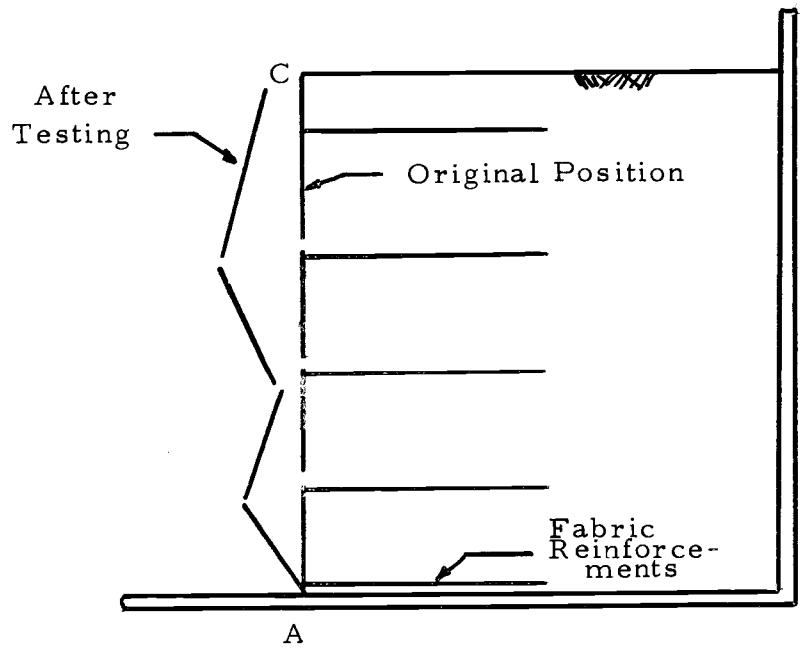

Figure 17. Deformation of plywood wall facing after testing.

Discussion of Results

The model tests showed that reinforced earth walls fail by the lateral movement of a failure wedge as predicted by the lateral stress theory. For an angle of internal friction of 38°, the Rankine lateral stress theory predicts that the failure plane will be located at $45^{\circ} + \phi/2$ from the horizontal or at 64°. The data in Table 6 show that most of the failure planes in the models were very close to this inclination. Examination of the fabric reinforcement after testing indicated that the fabric failed in most of the layers at the location of the failure plane. This does not agree with the lateral stress theory or the results of Lee's model tests. It does tend to correlate with the measurements taken by the California Division of Highways. The lateral stress theory assumed that the tensile force in the reinforcements would be a maximum at the wall face and would decrease to zero at the free end of the reinforcement. Thus breaking of the reinforcements should occur at the face first. For Test 2A, the failure plane passed through layer one 2.0 inches from the face, layer two 3.9 inches from the face, layer three 5.9 inches from the face and layer four 7.8 inches from the face. From Figure 16 it can be seen that layers one, two and three failed at approximately these distances from the face. Apparently layer four failed by pulling out rather than by breaking.

The lateral stress theory predicts that for a constant vertical spacing of the reinforcements, the maximum stress should occur in the lowest reinforcement in the wall. All of the models that failed by breaking of the reinforcements showed tearing in several of the lower layers. For a surcharge loading of q_f, the lateral stress theory predicts a stress distribution that increases with depth as shown in Figure 18 (a). The fact that all of the reinforcements showed tearing in the lower layers would indicate that the stress distribution reached a constant value behind the wall and may be as shown in Figure 18 (b).

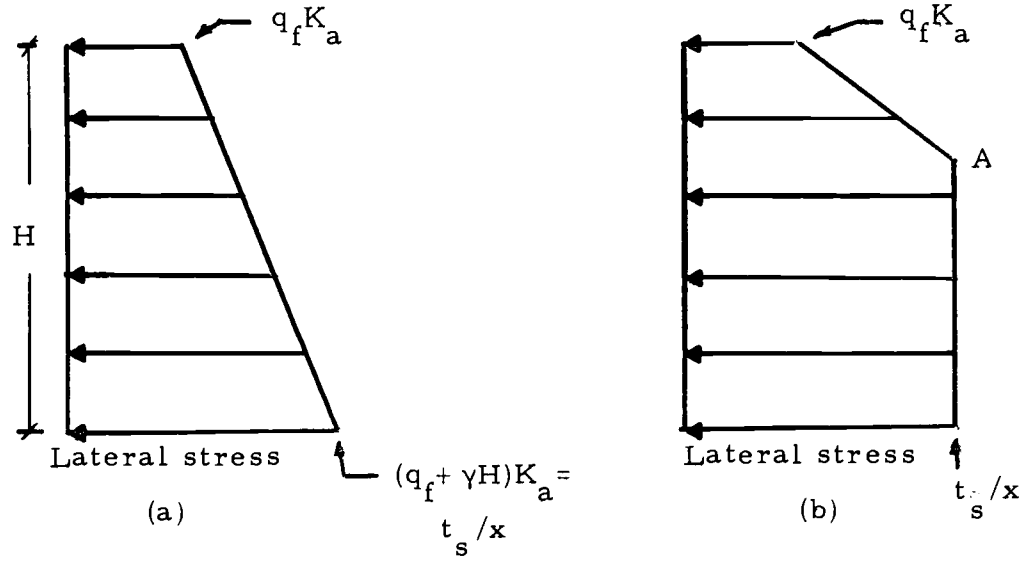

Figure 18. Stress distributions on reinforced earth walls at failure.

One possible explanation of the different stress distribution observed in this study might be the stress-strain characteristics of the reinforcement used. The fabric used in this study strained approximately 16 percent before failure. This elongation of the lower reinforcements may have allowed more of the upper reinforcements to develop their full tensile strength. The strain at failure for metal strap reinforcements is quite low and thus possibly the lower reinforcements would fail before the full tensile strength of the upper reinforcements was developed. It was impossible to determine the exact stress distribution behind the wall with the data that were measured in this study.

If t_s is defined as the strength of the fabric per unit width and q_f is the surcharge necessary to produce failure of the reinforced earth wall, the Rankine method predicts

$$q_f = \frac{t_s - \gamma H K_a X}{K_a X} \qquad [13]$$

If B is the width of the wall, the total lateral earth force resisted by the reinforcements will act horizontally and be given by

$$P = (1/2\ \gamma H^2 + qH)BK_a \qquad [14]$$

A free body diagram of the external forces acting on the failure wedge of a model reinforced earth wall is shown in Figure 19.

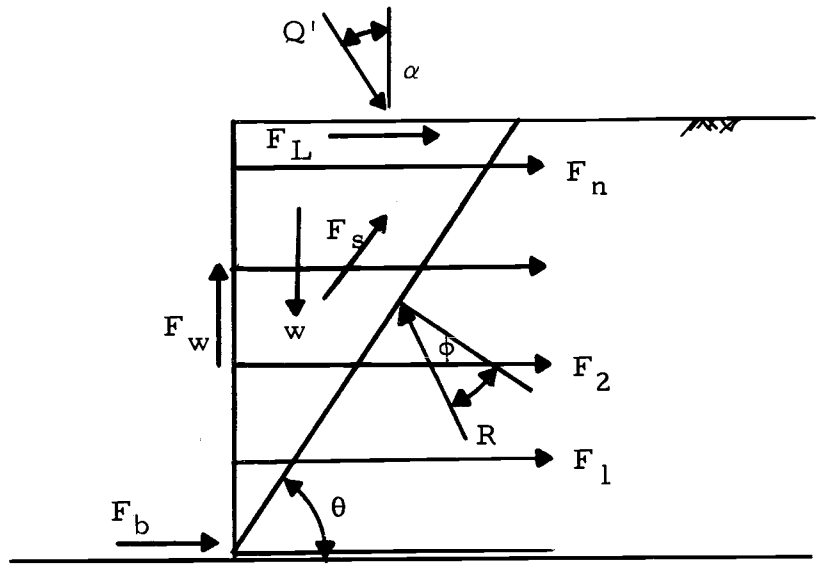

Figure 19. Forces acting on a failure wedge of a model reinforced earth wall.

The terms in Figure 19 are defined as follows:

Q' = Total inclined surcharge on failure wedge

W = Weight of failure wedge

F_b = Reaction at bottom of rigid-face wall due to friction

$F_{1, 2, \ldots n}$ = Forces in reinforcements

F_L = Loading plate friction

F_s = Sidewall friction

F_w = Friction between wall and soil

R = Resultant of normal and frictional forces on failure plane

ϕ = Angle of internal friction of soil

θ = Angle of inclination of failure plane

α = Surcharge inclination

The free body diagram shown in Figure 19 assumes that the sidewall friction acts parallel to the failure plane. The loading apparatus used to surcharge the models, measured only the vertical component of the surcharge or the force Q shown in Figure 20. At failure of the wall, the forces shown in Figure 19 may be represented by the force diagram shown in Figure 20. This force diagram assumes that the forces shown in Figure 19 that act directly on the wall, F_b, $F_{1,2,\ldots n}$, and F_w can be replaced by the total lateral earth force, P'. From Figure 20 it can be seen that if the other forces acting on the failure wedge can be estimated, it is possible to solve graphically for a value of the total force in the reinforcements. A comparison of the horizontal component of this total force with the value given by Equation 14 would indicate whether the lateral earth pressure theory correctly predicts the forces in the reinforcements. Table 7 lists the values of the theoretical lateral earth force calculated by each of the lateral stress theories and the actual force as determined graphically from the force diagram. The loading plate friction and sidewall friction used in determining the actual lateral earth force were calculated from the measured angles of friction.

Figure 21 shows a plot of the Rankine theoretical lateral force for failure versus the actual observed force for failure. The Rankine theoretical force was selected for comparison because in a full-sized

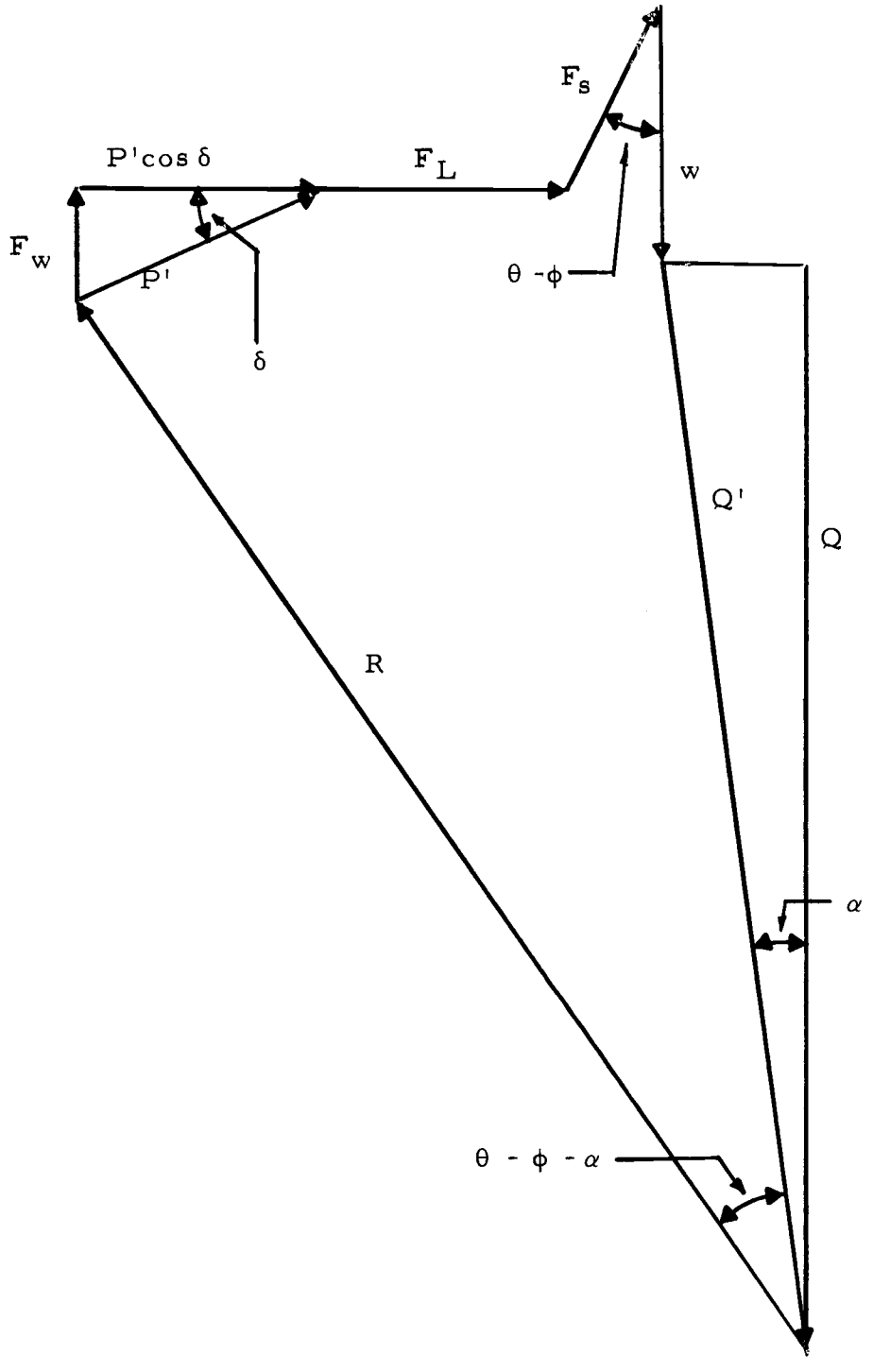

Figure 20. Force diagram for model failure wedge.

Table 7. Lateral earth forces resisted by reinforcements.

Model No.	Theoretical Values			Actual Value from Tests	Ratio
	Rankine Method	Coulomb Force Method	Coulomb Moment Method		
	P_1 (lb)	P_2 (lb)	P_3 (lb)	$P' \cos \delta$ (lb)	$P' \cos \delta / P_1$
1A	112	127	112	230	2.1
2A	121	140	121	208	1.7
3A	121	140	121	153	1.3
4A	121	140	121	155	1.3
5A	121	140	121	188	1.6
6A[a]	121	140	121	-	-
7A[b]	273	291	273	>512	>1.9
8A	273	291	273	328	1.2
9A	157	171	156	198	1.3
10A	341	356	341	391	1.2
11A[b]	250	273	222	>473	>1.9
12A	112	110	88	256	2.3
13A	112	110	88	270	2.4

[a]Pullout failure

[b]Model did not fail

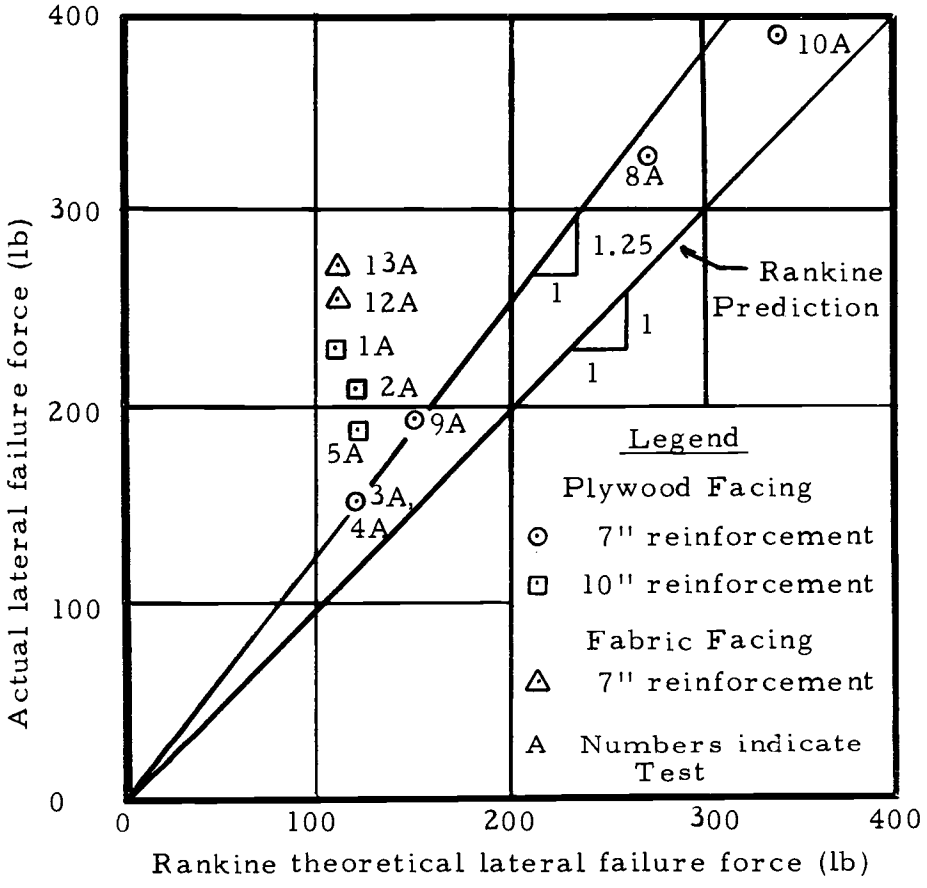

Figure 21. Rankine theoretical lateral failure load versus actual lateral failure load for models.

wall where the number of layers of reinforcement would be high, the Coulomb values would approach the Rankine value.

From Table 7 and Figure 21 it can be seen that for all of the tests performed, the model walls supported higher loads than any of the theories predicted. For the plywood-faced tests, if the models that did not fail are ignored and Test 1A is disregarded because of the loading plate configuration, the test results fall into two groups. Tests 3A, 4A, 8A, 9A, and 10A had seven inch reinforcement. For these five tests, the actual lateral force was 1.2 to 1.3 times the theoretical lateral force. Tests 2A and 5A with 10 inch reinforcement showed lateral forces 1.6 to 1.7 times the theoretical lateral force. The lateral stress theory predicts that the wall will fail when a failure is initiated in the lower-most reinforcement layer. As long as sufficient embeddment is achieved to prevent a pullout failure, the lateral stress theory does not predict a difference due to reinforcement length. One possible explanation for the higher observed lateral forces with longer reinforcement is that with the longer reinforcements, more layers crossed the failure plane. Thus if the failure wedge acted as a rigid body, the longer reinforcements would provide more restraint to lateral movement.

Models 12A and 13A were fabric-faced models and the actual failure loads on these models were considerably higher than predicted by the lateral stress theory. The lateral and vertical deformation of

these models was also considerably higher before failure than for the other models. The sand at the face of these models was loose compared to the sand in the backfill. The increase in strength for these models was apparently associated with the strength-deformation characteristics of the sand backfill. If the load that the sand could support increased with deformation, this would explain the higher observed failure loads. The failure mode for these tests was somewhat different than for the other tests in that tearing of the fabric occurred at both the face and the failure plane location.

Test 6A failed suddenly by pullout of the reinforcements and totally collapsed. Figure 22 shows the reinforcement arrangement for this model. The Rankine method computes a factor of safety against pullout at each reinforcement level by comparing the lateral pressure at that level to the frictional resistance of the portions of reinforcement behind the failure plane. The Coulomb methods consider the stability of the total wall and compute the factor of safety by comparing the total lateral force to the total resisting force or by comparing the total overturning moment about the toe to the total resisting moment about the toe.

Table 8 shows the calculated factors of safety by each of the three methods.

The Rankine method predicted failure of the model by pullout of the reinforcements above layer one before loads were applied. The

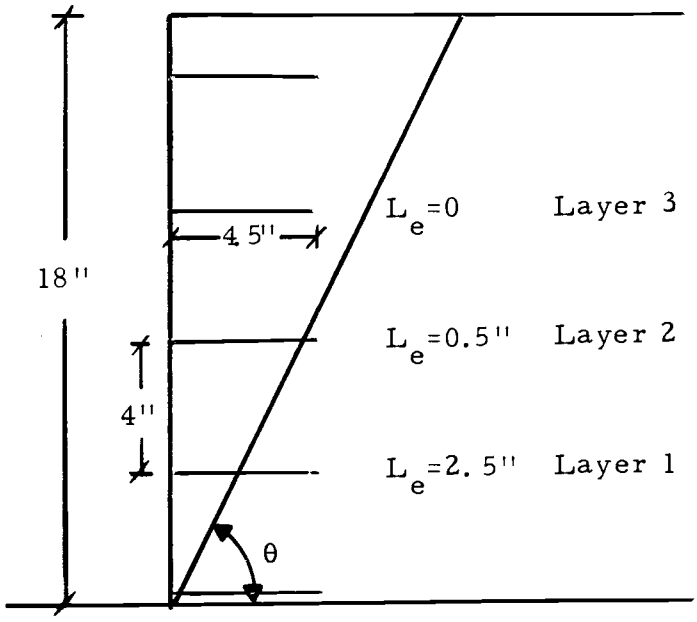

Figure 22. Reinforcement arrangement for Test 6A.

Table 8. Calculated factors of safety against pullout for Test 6A.

		Before Loading	At Failure Load
Rankine	Layer 1	2.0	2.0
	Layer 2	0.4	0.4
	Layer 3	0	0
Coulomb Force		1.8	1.5
Coulomb Moment		1.4	0.9

Coulomb moment method was the most accurate in predicting the pullout failure. As the load was applied, the factor of safety decreased from 1.4 to 0.9 at the time of failure.

The equivalent confining stress theory can possibly be used to explain the fact that tearing of the reinforcement generally occurred only in the lower layers. In the lower layers, the initial confining stress was apparently above the critical confining stress as shown in Figure 7. When these layers failed, the fabric was torn while in the higher layers the confining stress was below the critical confining stress and the layers failed by sliding between the fabric and the sand.

The fact that the models with 10 inch reinforcement failed at higher loads than the models with seven inch reinforcement can possibly be explained by the stress distribution shown in Figure 18. Point A in Figure 18 (b) represents the point at which the stress reaches a constant level behind the wall. For the models with 10 inch reinforcement, this point may be reached at a higher level on the wall than for the models with seven inch reinforcement. This would produce a higher lateral force on the wall.

As can be seen from the force diagram in Figure 20, there are many potential sources of error in the model testing and data analysis procedure used in this study. The force diagram solution for the lateral force is sensitive to variations in loading plate friction and insensitive to variations in sidewall friction. The errors introduced

by this analysis should be of similar magnitude for all tests and regardless of what the actual lateral force is, it can be seen that the models with 10 inch reinforcement supported higher loads than did the models with seven inch reinforcement and that the fabric-faced models supported higher loads than the plywood-faced models. The results of the model tests give a good indication of the effect of variations in model design but further study and possibly a redesign of the model apparatus needs to be undertaken before results can be strictly interpreted.

COMPARATIVE COST ANALYSIS

One of the basic requirements for the practical application of any new idea is that it must be economically feasible. Lee (5) has conducted a detailed economic comparison between metal strap reinforced earth walls and other retaining structures such as metal bin walls and cantilever reinforced concrete retaining walls. The results of his study are presented in Figure 23. It should be noted that the costs shown in Figure 23 are for 1971 and were calculated for the Southern California area.

From Figure 23, it can be seen that metal strap reinforced earth walls are quite economical compared with other conventional retaining structures.

It was not the purpose of this study to conduct a detailed economic analysis of fabric reinforced earth walls but a comparison between the cost of materials in a metal strap reinforced earth wall and a fabric reinforced earth wall was made. If it is assumed that construction methods and the cost of backfill are the same for fabric reinforced walls as for metal strap reinforced earth walls, the difference in cost between the two types will be determined by the difference in the cost of the facing and reinforcement elements for the two types. This assumption probably favors the metal strap reinforced earth wall because as stated previously, the construction methods would be expected to be simpler for a fabric reinforced earth

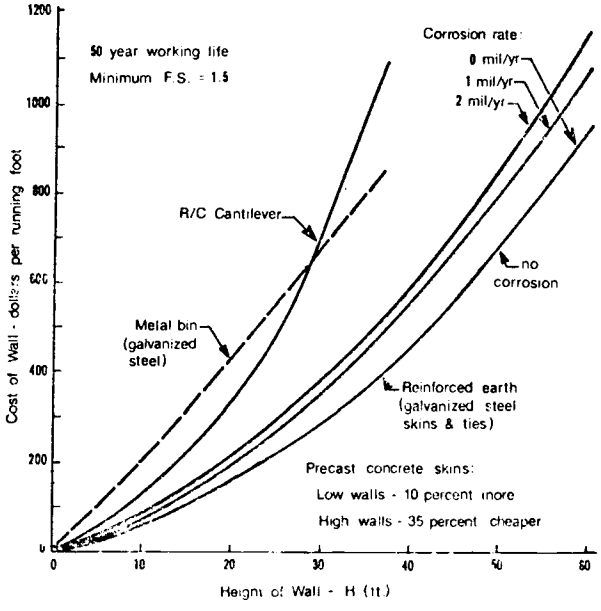

Figure 23. Comparative costs of different types of retaining structures (5).

wall. The fabric that was selected for the comparison was a non-woven polypropylene fabric that had an ultimate strength of 70 lb/in and a cost of $\$1.00/yd^2$. Table 9 shows a comparison between the costs of materials for metal strap reinforcements and fabric reinforcement.

Table 9. Costs of reinforcement materials for reinforced earth walls.

Wall Height (ft)	Price per Square Foot of Wall Surface ($)		Fabric Wall Vertical Reinforcement Spacing (ft)	Fabric Wall Reinforcement Length (ft)
	Metal Strap	Fabric		
5	-	0.45	2.5	3.1
10	5.00	0.66	2.0	5.3
15	5.50	0.96	1.5	7.5
20	6.00	1.50	1.0	9.6
30	7.00	-	-	-
40	8.00	-	-	-

The metal strap reinforcement costs listed in Table 9 are for walls with either steel or precast concrete facing and were obtained from the Reinforced Earth Company (12), which holds the patent rights to metal strap reinforced earth walls in the United States. The costs are for 1974 and include the cost of engineering and design of the structure and the cost of field supervision of construction. The actual cost of the materials would be less than these figures. The fabric costs were calculated for a fabric-faced reinforced earth wall designed by the Rankine method with a factor of safety of 1.5 with

respect to reinforcement breaking and 1.0 with respect to pullout for a typical granular backfill. Typical fabric spacing and embeddments so calculated are also shown in Table 9. These values are included for illustrative purposes only and are not intended as design guides. The costs are only for the fabric necessary for construction.

Comparison of the costs in Table 9 shows that fabric reinforced earth would probably be quite competitive at low wall heights. Calculations with the fabric used for this study show that for wall heights above 20 feet, the vertical fabric spacing is less than one foot. Construction methods would be limited with smaller fabric spacings and hence walls over 20 feet using this fabric may not be feasible. Feasible wall heights and material costs would depend on the fabric selected for construction and other details of the specific problem.

CONCLUSIONS

The concept of fabric reinforced earth retaining walls appears to be structurally feasible and economically attractive for low wall heights. Design procedures that have been applied to metal strap reinforced earth walls give conservative results when applied to fabric reinforced earth walls. Further investigation is needed to define the mechanism of fabric reinforced earth and to establish design methods. Some of the areas that need further investigation and some suggestions for further research are as follows:

1. The model apparatus used in this study needs to be redesigned to eliminate sources of friction and further model tests need to be run to confirm fabric reinforced earth behavior.
2. The actual stress distribution behind reinforced earth walls needs to be investigated. Instrumentation of model tests would define this distribution.
3. The construction and instrumentation of a full sized field model fabric reinforced earth wall would provide information that is more reliable than small scale model data.
4. A more accurate estimate of the costs of building fabric reinforced earth walls is needed. Fabrics other than polypropylene should be considered.

BIBLIOGRAPHY

1. Bowles, J. E., Foundation Analysis and Design, McGraw-Hill, Inc., New York, 1968, pp. 265-308.

2. Chang, J. C., Forsyth, R. A., and Beaton, J. L., "Performance of a Reinforced Earth Fill," Highway Research Report CA-DOT-TL-2115-1-74-04, California Department of Transportation, Division of Highways, Sacramento, Calif., Jan., 1974, 17 p.

3. Kelly, P. B., "Design and Evaluation of a Foundation Model Testing Device," Master's thesis, Oregon State University, Corvallis, 1969, 30 p.

4. Lazebnik, G. E., and Chernysheva, E. I., "Certain Errors in Experimental Determination of Earth Pressure on Models of Retaining Walls," Hydrotechnical Construction, No. 4, Apr., 1968, pp. 333-339.

5. Lee, K. L., Adams, B. D., and Vagneron, J. J., "Reinforced Earth Walls," Report No. 7233, University of California at Los Angeles School of Engineering and Applied Science, Apr., 1972, 219 p.

6. Lee, K. L., Adams, B. D., and Vagneron, J. J., "Reinforced Earth Retaining Walls," Journal of the Soil Mechanics and Foundations Division, ASCE, Vol. 99, No. SM10, Oct., 1973, pp. 745-764.

7. Terzaghi, K., and Peck, R. B., Soil Mechanics in Engineering Practice, 2nd ed., John Wiley & Sons, Inc., New York, 1967, pp. 184-267.

8. Vidal, H. C., United States Patent No. 3,421,326, Jan., 1969.

9. Vidal, H. C., "The Principal of Reinforced Earth," Highway Research Record, Highway Research Board, No. 282, 1969, pp. 1-16.

10. Walker, B. P., and Whitaker, T., "An Apparatus for Forming Uniform Beds of Sands for Model Foundation Tests," Geotechnique, Vol. 17, No. 2, 1967, pp. 161-167.

11. Yang, Z., "Strength and Deformation Characteristics of Reinforced Sand, "Doctor's thesis, University of California at Los Angeles, Los Angeles, 1972, 236 p.

12. _____, "More About Reinforced Earth," The Reinforced Earth Company, 1225 19th St. N.W., Washington, D.C., 1974, p. 4.

APPENDIX

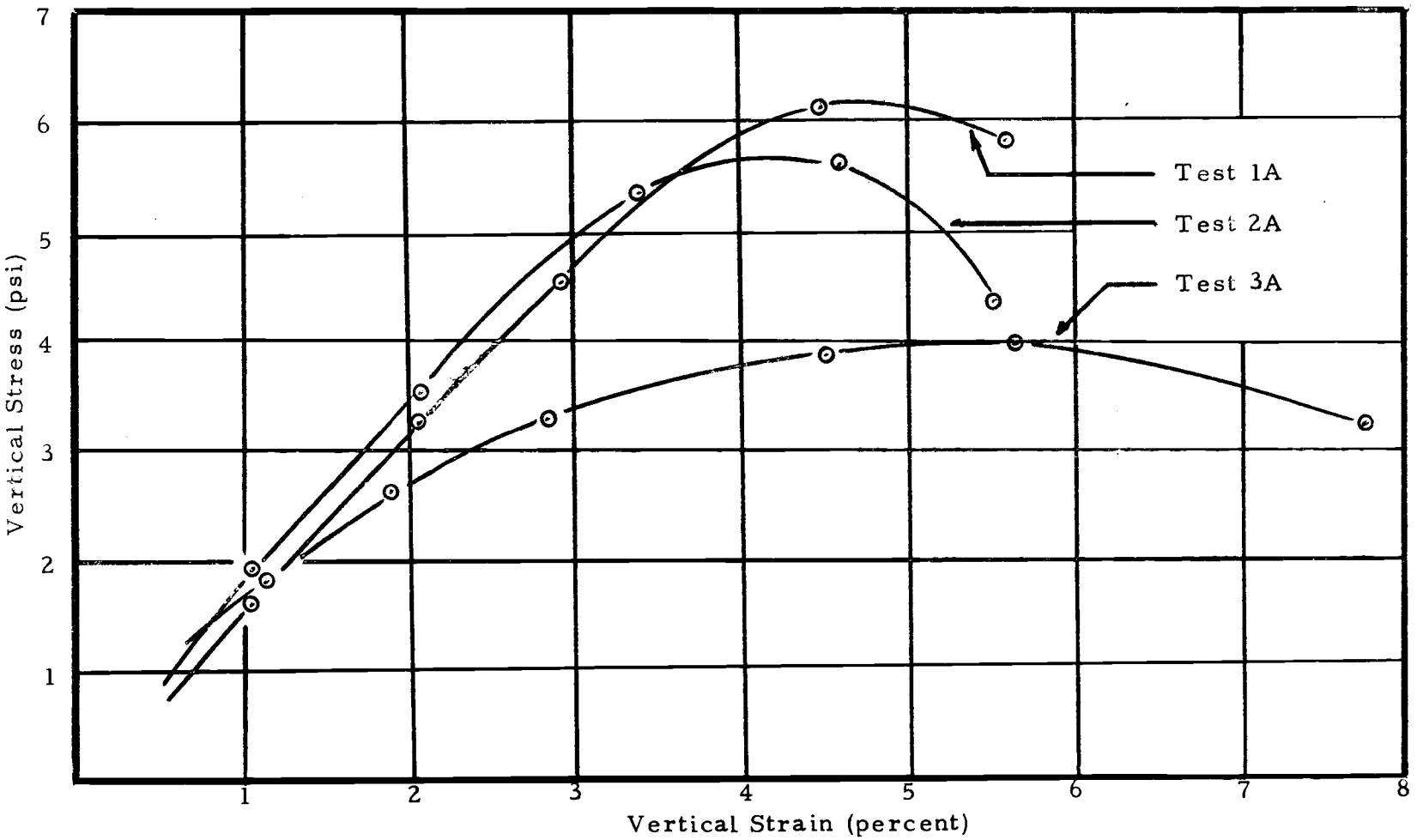

Figure 24. Stress-strain curves for Tests 1A, 2A, and 3A.

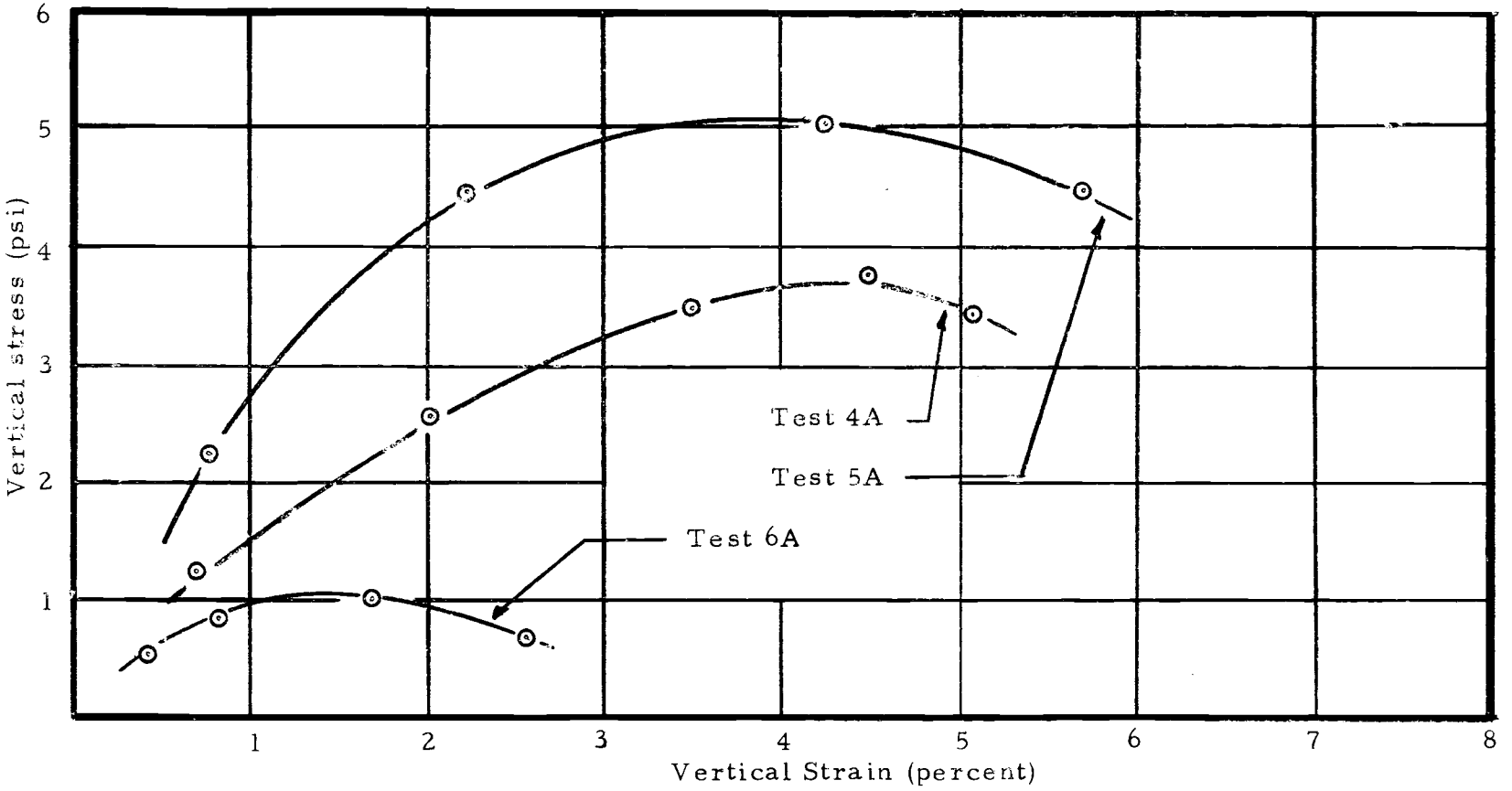

Figure 25. Stress-strain curves for Tests 4A, 5A, and 6A.

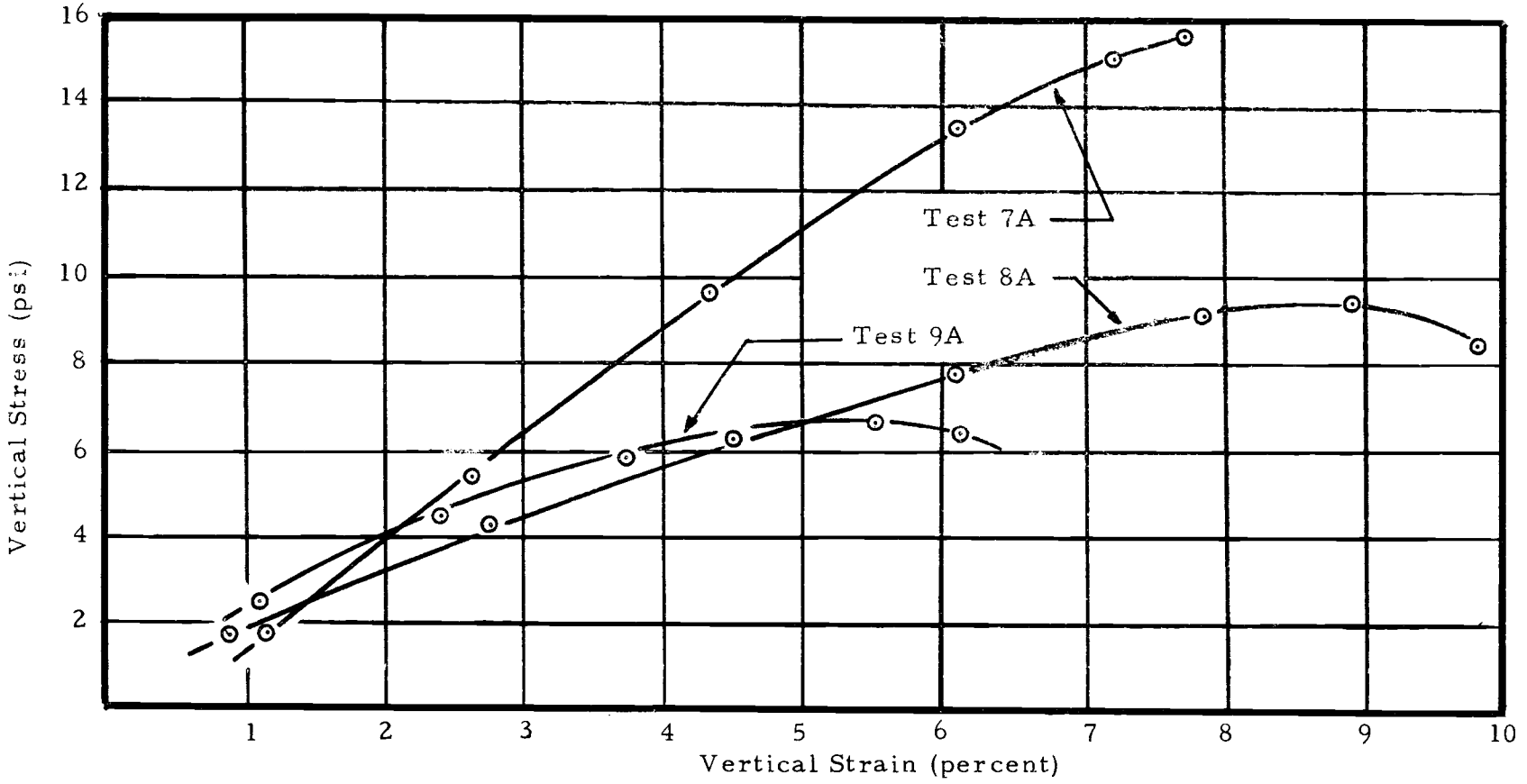

Figure 26. Stress-strain curves for Tests 7A, 8A, and 9A.

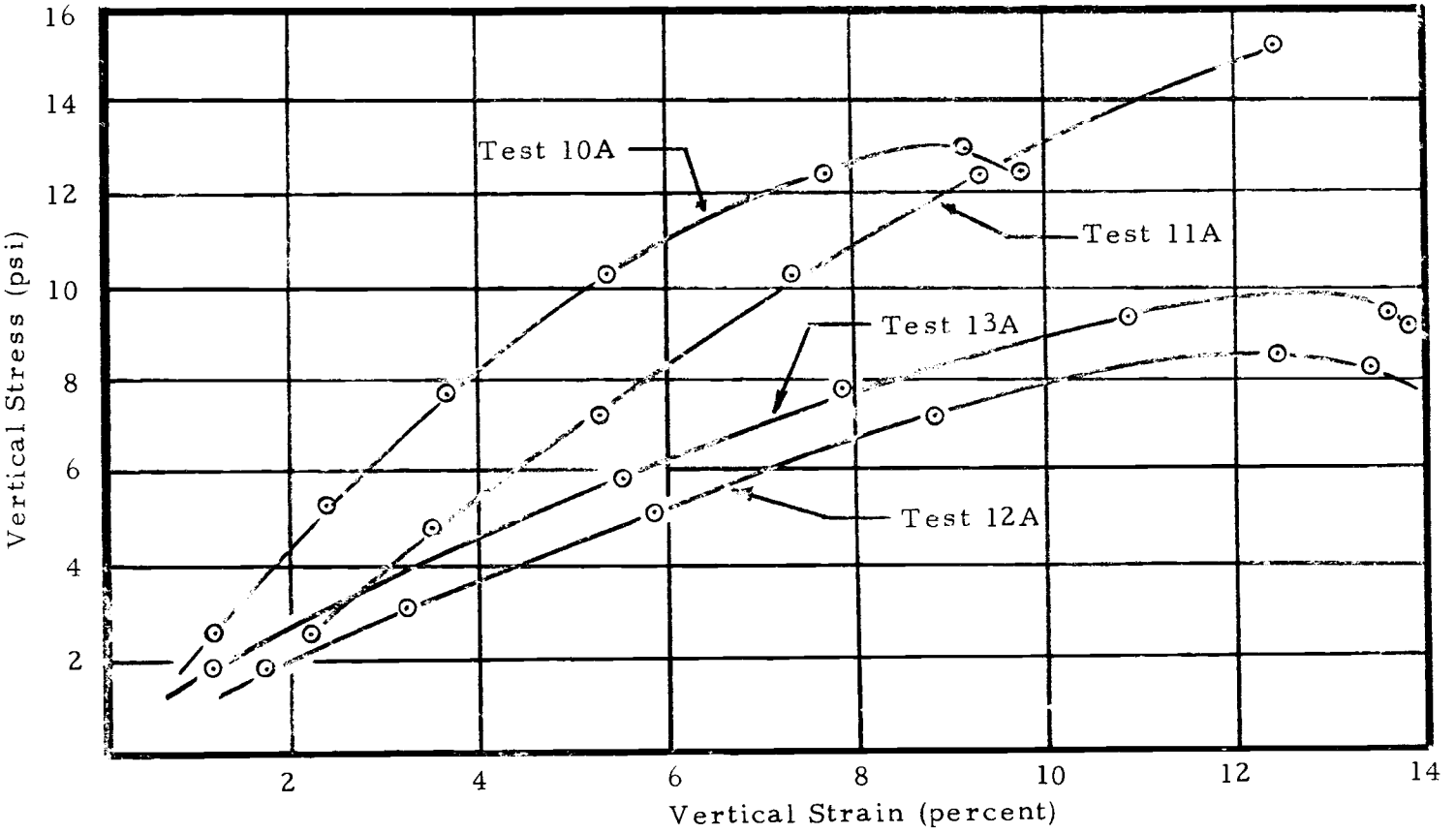

Figure 27. Stress-strain curves for Tests 10A, 11A, 12A, and 13A.